Proceedings of the ASME 2016 Dynamic Systems and Control Conference
DSCC2016
October 12-14, 2016, Minneapolis, Minnesota, USA

DSCC2016-9706

DYNAMIC MODELING OF A 2-DOF CABLE DRIVEN POWERED ANKLE-FOOT PROSTHESIS

Houman Dallali
Department of Mechanical Engineering, Engineering Mechanics
Michigan Technological University
Houghton, MI 49931- 1295
hdallali@mtu.edu

Evandro Ficanha
Department of Mechanical Engineering, Engineering Mechanics
Michigan Technological University
Houghton, MI 49931- 1295
emficanh@mtu.edu

Mohammad Rastgaar Aagaah
Department of Mechanical Engineering, Engineering Mechanics
Michigan Technological University
Houghton, MI 49931- 1295
rastgaar@mtu.edu

ABSTRACT

The first step to study and develop a two Degrees of Freedom (DOF) prosthesis is to derive a dynamic model for simulation and control design. In this paper, the ankle-foot prosthesis has controllable Dorsi-Plantarflexion (DP) and Inversion-Eversion (IE) DOF. We derive a compliant dynamic model for a recently developed ankle-foot prosthesis followed by identification of the actuators, transmission, and prosthetic foot parameters. The resulting model is then verified experimentally and in simulation. Dynamic decoupling of the actuators to the ankle's DP and IE DOF is also investigated using Bode plots. The code used for simulating the prosthesis is provided on GitHub for the community.

1 INTRODUCTION

Novel ankle-foot prostheses are providing increasing assistance to trans-tibial amputees [1,2]. Ankle-foot prostheses can be categorized into passive, semi-active and active devices. Commercially available prostheses at a suitable cost are typically passive and semi-active devices. Passive ankle-foot prostheses are developed with multi-axial rotation in three anatomical planes [3]. The semi-active devices, such as PROPRIO FOOT® (Össur, Reykjavik, Iceland) provide enhanced foot-ground clearance during the swing phase, reducing the risk of trips and falls [4]. This foot does not provide assistive propulsion to the gait during the stance or push off phases of walking. A recently developed foot called the Pro-Flex® provides assistive propulsion during push off with 27° ankle range of motion in DP [5]. These devices do not actively assist the user when navigating rough outdoor terrains or indoor slopes and stairs. These limitations are being addressed with active prostheses that are mainly being developed at research laboratories. Only in the last few years have a few commercial products become available [6]. Impedance control has been proposed as a suitable solution for the control of active prostheses, providing improved physical interaction with the environment [7].

The design of a 2 DOF ankle-foot prosthesis (SPARKy 3) was proposed by Bellman, et. al. [8] which was based on the design of Sparky, a one DOF ankle foot prosthesis [9]. The authors have developed a cable driven ankle-foot prosthesis (Fig.1) with two controllable DOF of the ankle in the sagittal and frontal planes [10]. The design [11] using Bowden cables to deliver power to the ankle, allowing a quite compact design that is lightweight to wear (3 kg total weight), while offering desired impedance in two main directions of the human ankle that is DP and IE. Panzenbeck and Klute [12] developed a 2 DOF ankle-foot prosthesis which has powered inversion-eversion DOF while DP is equipped with a passive spring. Recently, an ankle-foot emulator with off-board motors capable of actuating the ankle joint in DP and IE was developed by Collins et. al. [13]. This system also uses Bowden cables to deliver motor torque to the ankle-foot device.

The use of Bowden cables, however, comes at its own cost of increasing the complexity of the control system. Both the Bowden cables and the gearboxes have about 30% friction loss

[14, 15]. The variation in the cable pretension might lead to a more compliant transmission and must be taken into consideration during the design of the controller. In this paper, we address these issues by introducing a compliant model to capture the nonlinearity and parameter uncertainty. The model is used to study the effects of disturbances, while the prosthesis interacts with the environment, on the control system.

The paper is organized as follows. Section 2 provides a brief introduction to the ankle-foot prosthesis hardware design, the kinematics and dynamic model. Section 3 presents a series of tests designed to identify the friction model parameters and inertia of the actuators, transmission and the prosthetic foot. Section 4 uses the identified parameters with experimental data to validate the model. Section 5 analyzes the effect of the pulley radii and cable stiffness on the full dynamic decoupling of the ankle-foot prosthesis. Section 7 presents simulations of the ankle-foot system while interacting with the environment. The simulations results are verified experimentally. Finally, the paper draws conclusions and points out the future directions.

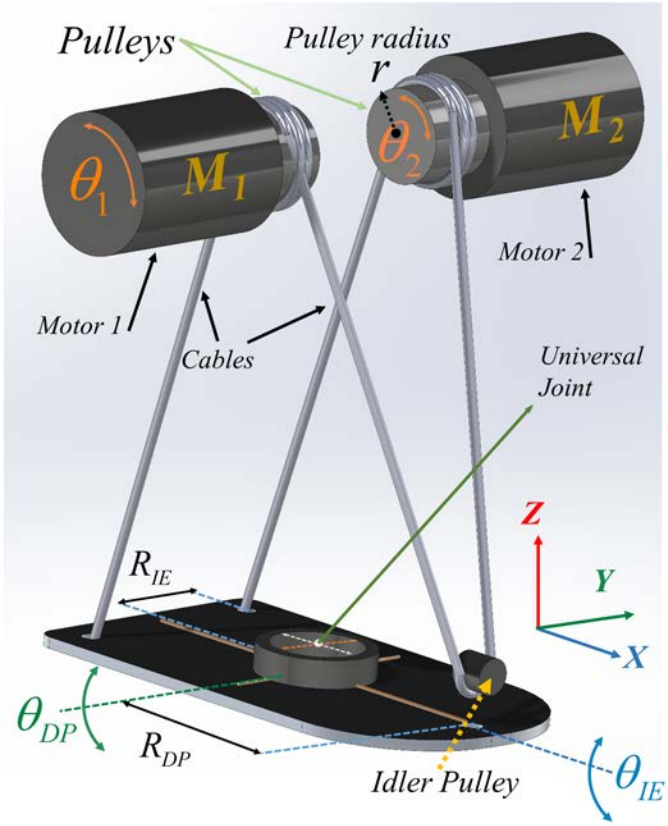

FIGURE 1: Schematics of a two-DOF cable driven mechanism used in the ankle-foot prosthesis.

2 MODELING THE ANKLE-FOOT PROSTHESIS

This section presents the kinematic (section 2.1) and dynamic equations (section 2.2) of the ankle-foot prosthesis. The state space model for the linearized system is also derived and used for the system analysis in sections 5 and 7.

2.1 ANKLE-FOOT KINEMATICS

The kinematic relationship between the two motor angles, θ_1 and θ_2, pulley radii, r, and the ankle DP and IE positions, θ_{DP} and θ_{IE} are

$$\theta_{DP} = \frac{r(\theta_1+\theta_2)}{2R_{DP}} \quad \theta_{IE} = \frac{r(\theta_1-\theta_2)}{2R_{IE}} \tag{1}$$

where R_{DP} and R_{IE} are distances from the centre of ankle joint to the cable attachment points in the sagittal and lateral planes (Fig.1). In DP motion, both cables and motors (M_1 and M_2) move in the same direction, while in IE they move in opposite directions. In the sagittal plane, two cables are active in moving the foot, while in the lateral plane only one cable is applying the force since the frontal part has an idler pulley. Hence, the stiffness in DP is twice the stiffness in IE. The inverse relationship between the motor angles and foot angles is

$$\begin{bmatrix}\theta_1\\ \theta_2\end{bmatrix} = \frac{1}{r}\begin{bmatrix}R_{DP} & R_{IE}\\ R_{DP} & -R_{IE}\end{bmatrix}\begin{bmatrix}\theta_{DP}\\ \theta_{IE}\end{bmatrix}, \quad \theta_m = R\theta \tag{2}$$

where $\theta = [\theta_{DP},\ \theta_{IE}]^T$, $\theta_m = [\theta_1,\ \theta_2]^T$ are the ankle and motor positions. The motor positions are reflected to the output of the gearbox using the 81:1 reduction ratio. The range of motion for the ankle joint in both DP and IE is ± 40 degrees only being constrained by software limits. The kinematic equations given in Eq.(1) and Eq.(2) assume infinitely stiff cables, but in the prosthesis the deflections due to finite cable stiffness creates transient dynamics. This effect is captured with the model presented next.

2.2 DYNAMIC MODEL

The nonlinear model of the ankle-foot prosthesis is represented in Eq.(3).

$$M\ddot{\theta} + \mathbf{c}(\dot{\theta},\theta) + \mathbf{g}(\theta) = K\left(R^{-1}\theta_{\mathbf{m}} - \theta\right) + \tau_d \tag{3}$$

$$J\ddot{\theta}_{\mathbf{m}} + D\dot{\theta}_{\mathbf{m}} + kr^2\left(\theta_{\mathbf{m}} - R\theta\right) = \tau_m - \tau_F \tag{4}$$

The rigid body equations are coupled to the motors via cables and pulleys where the matrices $M, \mathbf{c}, \mathbf{g}$ are mass-inertia, Coriolis/centripetal, and gravitational terms, respectively. R is the differential coupling between the motor and the links, K is the equivalent stiffness, and k is the stiffness of the cable. τ_d, τ_m, τ_F are link disturbance, motor, and frictional torques, respectively. Figure 1 shows the two motors driving the ankle using Bowden cables. The model matrices of actuator inertias, dampings and stiffness are

$$J = \begin{bmatrix}J_1 & 0\\ 0 & J_2\end{bmatrix}, D = \begin{bmatrix}d_1 & 0\\ 0 & d_2\end{bmatrix}, K = \begin{bmatrix}2kR_{DP}^2 & 0\\ 0 & kR_{IE}^2\end{bmatrix}. \tag{5}$$

The environment and ground reaction torques (τ_d) acting on the prosthetic foot can be simulated to investigate robustness of the controller designs. The proposed compliant model is based on the elastic joint robot model first proposed in [16]. The differential drive, cables and pulleys are also modeled for the prosthesis. In order to perform linear analysis on the model, Eq.(3) is linearized about the zero position and zero velocity equilibrium and the following state space system is derived in Eq.(6)

$$\begin{cases} \dot{x} = Ax + Bu & x = [\theta, \theta_m, \dot{\theta}, \dot{\theta}_m]^T \\ y = Cx + Du & u = [\tau_d,\ \tau_m]^T \end{cases} \tag{6}$$

$$A = \begin{bmatrix} 0_4 & I_4 \\ -A_1^{-1}(A_3 - A_4) & -A_1^{-1}A_2 \end{bmatrix}, B = \begin{bmatrix} 0_4 \\ -A_1^{-1}B_1 \end{bmatrix}, B_1 = \begin{bmatrix} I_2 & 0 \\ 0 & R \end{bmatrix}$$

$$A_1 = \begin{bmatrix} M & 0 \\ 0 & J \end{bmatrix} A_2 = \begin{bmatrix} 0 & 0 \\ 0 & D \end{bmatrix} A_3 = \begin{bmatrix} G & 0 \\ 0 & 0 \end{bmatrix} A_4 = \begin{bmatrix} -K & KR^{-1} \\ kr^2R & -kr^2I_2 \end{bmatrix}$$

where, I_n denotes an identity matrix of size n and $G = \frac{\partial \mathbf{g}}{\partial \theta}$ is the linearized gravity matrix. The next section discusses parameter estimation of this model using experimental data.

3 PHYSICAL PARAMETER ESTIMATION

In order to derive an accurate model capable of predicting the ankle-foot behavior in simulations, the actuator inertia, damping and friction are identified using experimental data. The parameters estimated in this section have physical interpretations as opposed to black box parameter identification methods [17].

First, the motors were disconnected from the Bowden cables and the foot to provide independent motor identification. The nominal parameters of the motor and gearbox can be derived from the manufacturer datasheet (see Table 1). The equation describing the motor dynamics is

$$J\ddot{\theta}_\mathbf{m} + D\dot{\theta}_\mathbf{m} = \tau - \tau_F \tag{7}$$

where τ_F represents the basic friction terms such as Coulomb and viscous which denote the presliding and sliding friction regimes [18, 19]. The amount of friction in the presliding regime is referred to as the static friction, or stiction, discussed in section 3.1, and the level of friction in sliding regime is called viscous friction which is discussed in section 3.2. Also the combined rotor, gearbox and pulley inertia is estimated in section 3.3.

Second, the Bowden cable stiffness, the mass-inertia and centre of mass (COM) of the prosthetic foot were derived based on theoretical calculations and CAD software.

3.1 STICTION IDENTIFICATION

Stiction can deteriorate the controller performance. Identifying the amount of stiction in the actuators can help compensating for these losses in the controller design. The model used here does not include the Stribeck effect but the asymmetry is considered. Hence, to quantify stiction, a periodic sawtooth current command with clockwise (CW) and counterclockwise (CCW) ramps were applied to the motor and the amount of current required to make the motor move was recorded in each experiment. Figure 2 illustrates these experiments while the motor amplifiers with integrated Proportional Integral (PI) current control were used. Using the nominal torque constant of the motors (1.66 Nm/A) the amount of stiction torque were $k_c^+ = k_c^- = 0.28$ in CW and CCW directions.

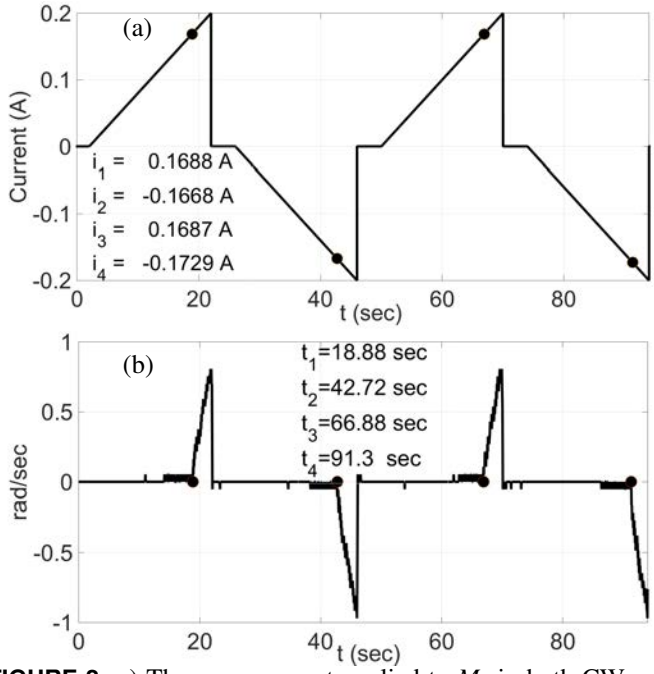

FIGURE 2: a) The ramp current applied to M_1 in both CW and CCW directions and b) velocity measurements during the stiction estimation experiment. The black circles indicate the times motor started to move.

3.2 VISCOUS FRICTION IDENTIFICATION

In addition to the motor damping D, the friction of the gearbox τ_F can be described in two forms: a simpler one being $\tau_F = k_v\dot{\theta}_m$, where k_v is the symmetric viscous friction coefficient, and a more accurate model having asymmetric viscous and Coulomb friction coefficients is

$$\tau_F = k_v^+\dot{\theta}_m + \left(k_v^- - k_v^+\right) f_1(\dot{\theta}_m) + k_c^+ + \left(k_c^- - k_c^+\right) f_2\left(\dot{\theta}_m\right) \tag{8}$$

where $k_c^{+/-}$ are the asymmetric Coulomb friction coefficients and $f_1\left(\dot{\theta}_m\right) = \dot{\theta}_m$, $f_2\left(\dot{\theta}_m\right) = 1$ when $\dot{\theta}_m < 0$ and zero otherwise. In the simulation in section 7, the symmetric Coulomb and viscous friction model is chosen, because the amount of asymmetry is negligible. Having identified the amount of stiction in the motor, one can design a velocity controller moving the motor at a constant velocity (zero acceleration) to identify viscous friction without exciting the inertia. In this experiment, a PI velocity controller was designed to track a number of velocities (3, 5 and 8 rad/sec) in both directions to identify the amount of viscous

TABLE 1: NOMINAL AND IDENTIFIED MOTOR DYNAMIC PARAMETERS (REFLECTED TO THE LOAD SIDE, SD: Standard Deviation).

Parameter	J	D (k_v)	k_c^+	k_c^-
Units	kgm^2	Nms	Nm	Nm
Nominal	0.028	0.02	0	0
Identified	0.048	0.112	0.28	0.28
SD	$\pm$ 0.002	$\pm$ 0.01	$\pm$ 0.01	$\pm$ 0.01

friction. The experimental results for CW/CCW velocity commands are shown in Fig.3. Given the nominal torque constant being $k_t = 1.66\ \frac{Nm}{A}$, the motor torques were -0.43, -0.63 and -0.80 Nm for CW direction and 0.45, 0.63 and 0.83 Nm for the CCW direction. Hence, the average viscous friction coefficient for CW is $k_v^+ = 0.114$ and for CCW is $k_v^- = 0.110$. Since the asymmetry is negligible, an average symmetric coefficient can be used $k_v = 0.112$.

3.3 ACTUATOR INERTIA IDENTIFICATION

The goal of this experiment was to measure the resulting velocity given the applied step torque command. In order to identify the combined inertia of rotor, gearbox, bearings and the pulley of an actuator, a step torque command was applied to the motor. The transfer function relating the input motor torque to the output velocity is

$$\frac{\dot{\theta}}{\tau_m} = \frac{1}{Js + D} \tag{9}$$

where the parameters J and D are to be estimated. The viscous damping coefficient is already estimated, that is $D = k_v = 0.112$.

The motor velocity is computed with differentiation of the position without any filtering. Having derived the velocity and knowing the input motor torque, one can use nonlinear least squares algorithm available from *Simulink®* parameter estimation toolbox. The initial guess for the inertia is based on the motor and gearbox manufacturer datasheet indicating a total reflected inertia of $J = 0.0248\ kgm^2$. The identified inertia is larger than the initial guess due to the inertia of the output pulleys, screws and bearings that rotate with the motors. The initial guess for the damping parameter is based on the viscous coefficient $k_v = 0.112$ derived in section 3.2. The optimization converges in four iterations as shown in Fig.4a. The step response of the identified model is compared to the experimental data in Fig.4b. The identified actuator parameters are shown in Table 1.

3.4 STIFFNESS ESTIMATION

The cable stiffness was estimated to be $218.8\frac{N}{mm}$ using $k = \frac{EA}{L} = 218.8\left(\frac{N}{mm}\right)$, where the Young modulus is $E = 196.5 \times 10^5\ Pa$ and the cable cross section is $A = 1.1135 \times 10^{-6}\ m^2$.

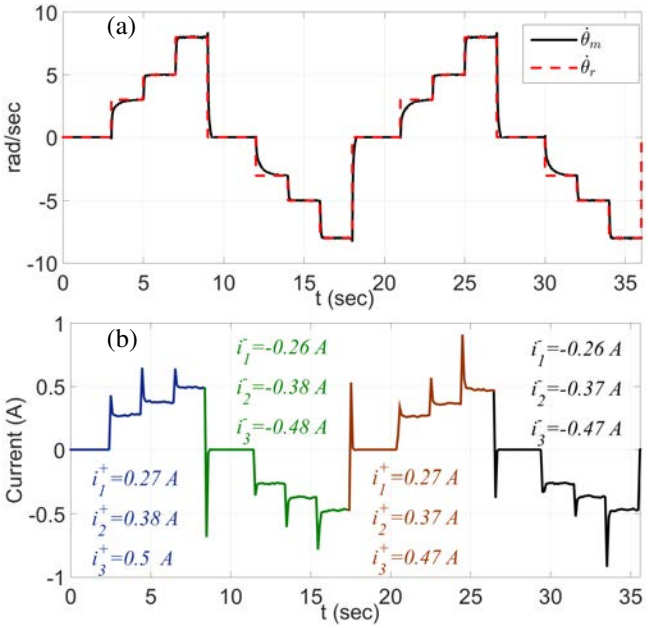

FIGURE 3: a) The velocity commands in both CW and CCW directions and b) the corresponding motor currents.

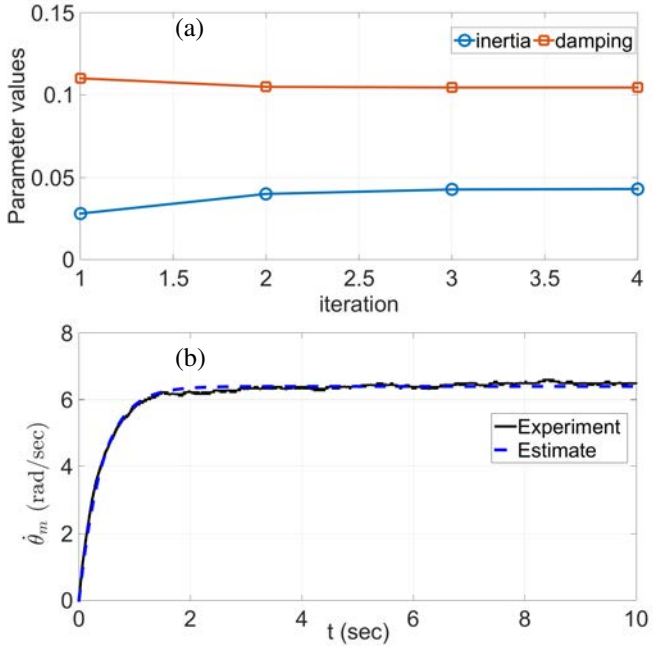

FIGURE 4: Identification results of the actuator. a) Parameter values of inertia and damping convergence to 0.048 kgm^2 and 0.112 Nms, respectively, using nonlinear least squares optimization. b) The experimental (Exp) and estimated (Est) step responses.

3.5 FOOT PARAMETER ESTIMATION

In order to estimate inertia values, the cables were detached from the universal joint and the inertia was estimated using CAD

software. The prosthetic foot dimension and mass parameters were measured as $33 \times 67 \times 228\ mm^3$ and mass of $0.425\ kg$. The result is shown in Table 2 and the foot CAD model is also shown in Fig.5.

TABLE 2: FOOT MASS INERTIA PARAMETERS. COM AND INERTIA ARE WITH RESPECT TO THE ANKLE JOINT AXES.

	M (kg)	COM (m)	I (kgm^2)
DP	0.465	0.0069	$I_z = 3.7486 \times 10^{-3}$
IE	0.465	0.0	$I_x = 9.3452 \times 10^{-4}$

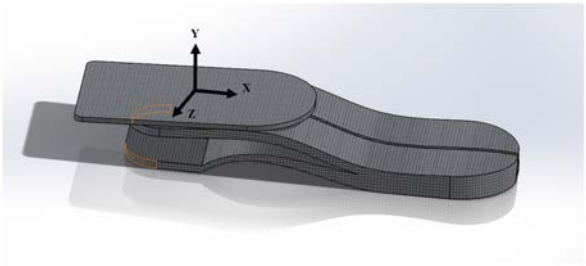

FIGURE 5: CAD model of the prosthetic foot used for inertia estimation.

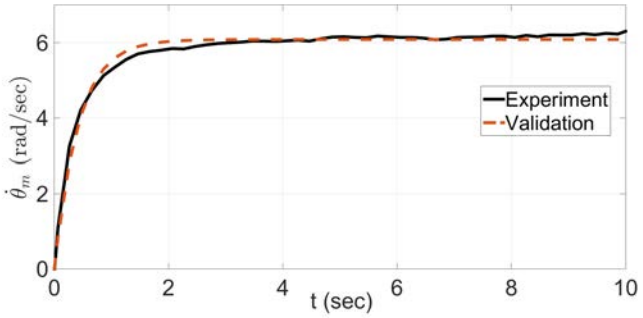

FIGURE 6: Actuator model validation using a torque step response. validation response is the dashed line and the new experiment is the solid line.

4 MODEL VALIDATION

Parameters with small standard deviations (SD) were derived for the dynamic model. A range of additional validation commands, such as step torque and sine position inputs, were applied to the model and the ankle-foot prosthesis and the comparison between the two are presented in this section.

4.1 ACTUATOR MODEL VALIDATION

In this section, the open loop motor model is compared to the *Maxon*® EC-4pole brushless DC motor powering the ankle-foot prosthesis. A step torque was applied to the motors and the comparison is shown in Fig.6. The model validation graph is compared to new experimental data in Fig.6.

4.2 ANKLE-FOOT MODEL VALIDATION

To validate the accuracy of the overall model, a set of sine waves were commanded to the motors and joint positions were recorded for comparison with the model (Fig.7). The PD controller used in the experiment and simulation had $k_p = 80$ Nm/rad and $k_d = 0.3$ Nms/rad for both motors. The motor and ankle positions have a good agreement with the proposed model. This test was repeated at different frequencies and similar results were derived.

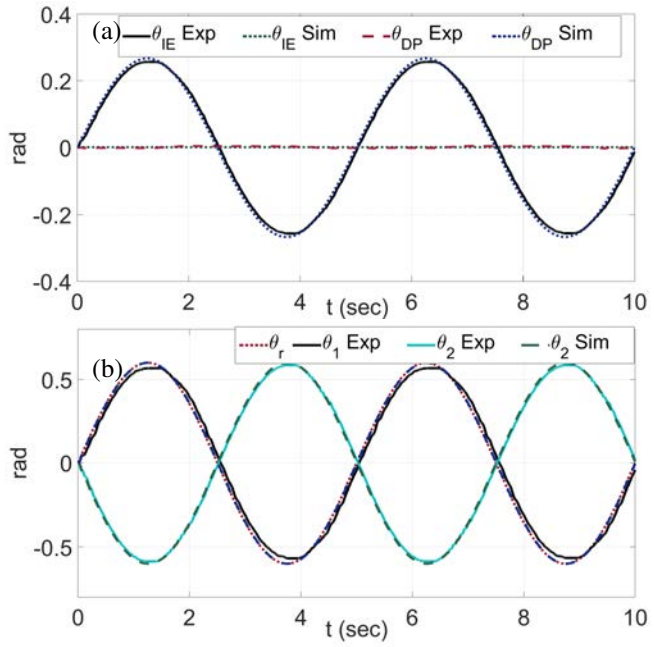

FIGURE 7: a) The sinusoidal position tracking at the IE DOF of the ankle and b) the corresponding motor positions. On the legends, Exp is experimental data and Sim is simulation.

5 DYNAMIC DECOUPLING

Open loop frequency response of the differential drive given in Eq.(6) was used to study the dynamic behavior of the ankle-foot prosthesis. The ratio between the motor and ankle lever arms ($r,\ R_{DP}, R_{IE}$), the ratio between the ankle lever arms in DP and IE (R_{DP}, R_{IE}), and the cable stiffness all have implications on the dynamic behavior of the prosthesis that can be explored using the open loop frequency response.

One design question that can be answered from the design point of view is what ratio to choose for the ankle lever arms (R_{DP} and R_{IE}) and pulley radii (r). Assuming a unit ratio of the pulleys to ankle lever arms, decoupling was analyzed using Bode plots. The ankle joint in DP had twice the stiffness relative to the IE. In Fig.8, the resonance of load velocity and the anti-resonance of the motor velocity, which are a function of cable stiffness and the ratio between the foot and the motor inertias, are depicted. In the ankle-foot prosthesis the load-inertia is smaller compared to the reflected motor and gear inertia improving the resonance effects.

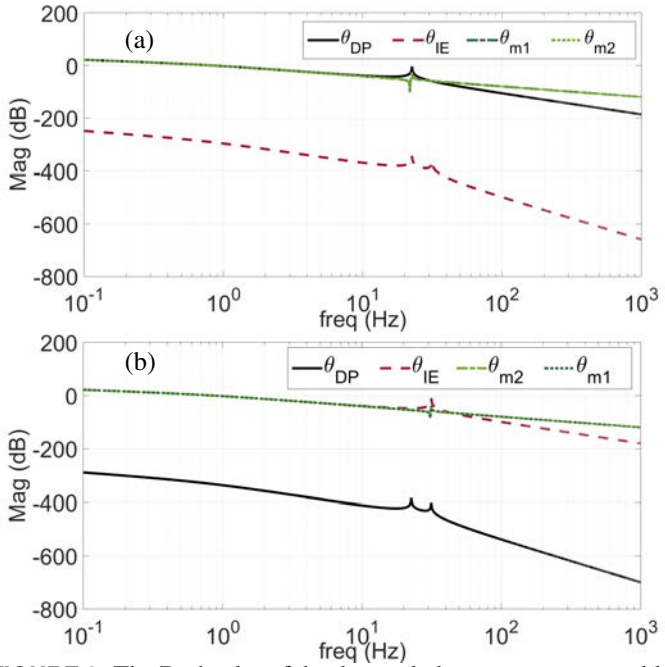

FIGURE 8: The Bode plot of the decoupled motor torque to ankle and motor positions, when ratio between pulley radii and ankle lever arms are in unity. a) θ_{DP} and b) θ_{IE} were independently controlled in open loop using Eq.(6).

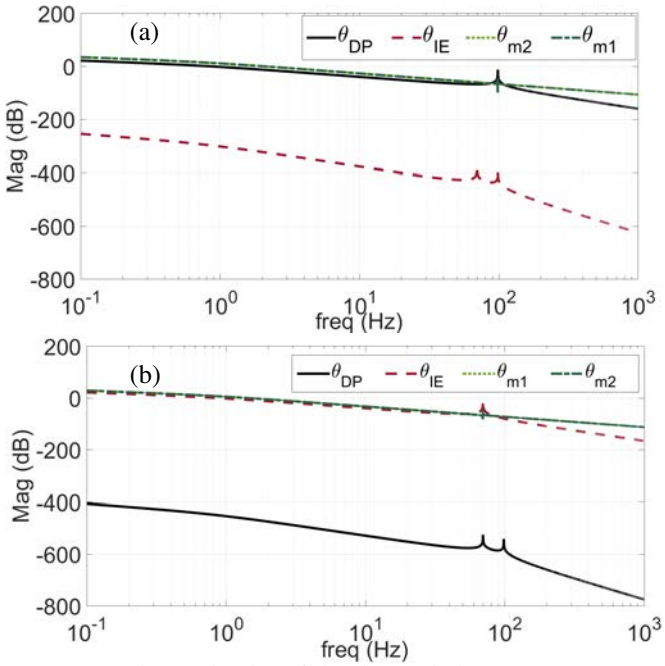

FIGURE 9: The Bode plot of the decoupled motor torque to ankle and motor positions, with actual ratio between pulley radii and ankle lever arms. a) θ_{DP} and b) θ_{IE} were independently controlled in open loop using Eq.(6). The kinematic difference between motor and ankle positions due to the ratio of pulley and the lever arms is evident.

Remarkably, a full decoupling between the input DP torque and DP position from the IE DOF was achieved. This is evident from the Bode plots, showing that both motor positions have the same magnitude as the DP (Fig.8a) or IE (Fig.8b) position depending on the input applied in DP or IE. Decoupling is valid until the resonance occurs at 23 Hz for DP and 31 Hz for IE. Note that these resonance frequencies are a result of both the stiffness and mass-inertia of the foot.

Introducing the actual difference between the pulley radii and the ankle feet lever arms, 13 dB attenuation in DP and 8 dB attenuation in IE are shown between the ankle positions and motors in Fig.9. This trend can be further analyzed by testing various sizes of lever arms at the ankle with respect to the pulley radii.

To achieve full decoupling, a dynamic compensator in the closed loop can be introduced. In addition, the cable stiffness also plays a role in the feasible closed loop bandwidth limited by the resonance frequency. In simulation, the cable stiffness was reduced by a factor of ten changing the resonant frequency from 23 Hz to 7.5 Hz in DP and 30 to 3.2 Hz in IE (Fig.10). In the actual experiment, when suitable pretension is applied to the cable, the stiffness can be increased sufficiently.

6 TORQUE CONTROL

In order to implement motor side impedance control, ESCON module 50/5 motor amplifiers with integrated current control were used for motor torque control. External forces were measured via the strain gauges that are mounted on the foot. When applying impedance control at the ankle, the torque at the DP and IE DOF should be controlled through the cable and pulley transmission.

It is of interest to derive the open loop Bode plot from the decoupled motor inputs to the DP and IE joint torques. Based on the model given by Eq.(3), the joint torques at the ankle DP and IE are given in Eq.(10) which was used in the state space model given in Eq.(6) by changing the output matrix C to give joint torque. The resulting Bode plots are shown in Fig.11. Providing suitable pretension of the cable and assuming the nominal stiffness, the resonance in DP is 98 Hz and in IE it is 70 Hz. It should be noted that these plots were produced for identical motors and the angle-dependent friction of the cables was not considered. In future work, a dynamic torque controller should be designed to cancel all the model and prosthesis discrepancies and provide the desired torque at the ankle.

$$\tau_j = K\left(R^{-1}\theta_m - \theta\right) \tag{10}$$

7 SIMULATION AND EXPERIMENTAL RESULTS

The simulation code based on $Matlab - Simulink^{®}$ is presented online [20]. This simulation can be used for initial control development and simulation as well as having the option to switch the controller from the model to the actual hardware us-

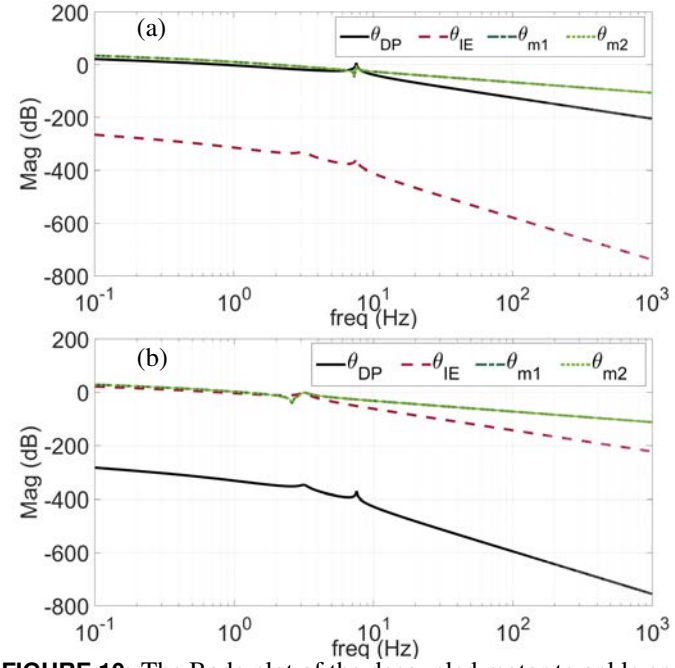

FIGURE 10: The Bode plot of the decoupled motor to ankle and motor positions, with actual ratio between pulley radii and ankle lever arms. Cable stiffness was reduced by 10 times. a) θ_{DP} and b) θ_{IE} were independently controlled in open loop using Eq.(6).

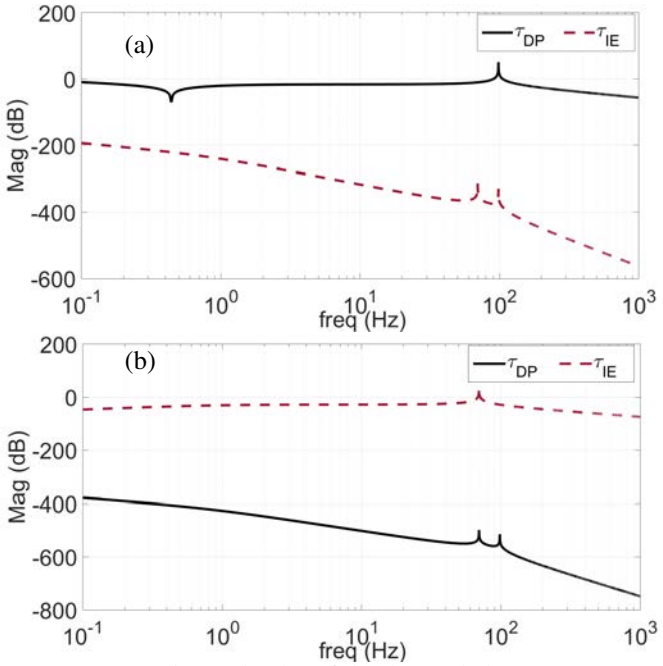

FIGURE 11: a) The Bode plot of the decoupled motor torques to ankle DP and b) to ankle IE torques.

ing the *Simulink*® real-time. The open loop model without control cannot deal with disturbances or parameter uncertainties. A simple PD control was added to the motor side in the model for tracking and disturbance rejection simulation. The PD control law is

$$u = k_p(\theta_r - \theta_m) - k_d\theta_m \tag{11}$$

where $k_p = 90$ Nm/rad and $k_d = 5$ Nms/rad for both motors in simulations and experiments. The motor position was measured using E4T OEM Miniature Optical Encoder from *US Digital*®. They are installed on the motor shaft before the gearbox. Quantization noise due to the encoder resolution (53.8680 microradians, equivalent to 116640 pulses/revolution at the output of the gearbox with 81:1 ratio) was added to the simulation for velocity estimation. In addition, the Coulomb (0.28 and -0.28 Nm in CW and CCW directions, respectively) and viscous friction (viscous coefficient of 0.112 in both CW and CCW directions) were added to the model to capture the friction loss in actuation and transmission. The model and control block diagram is shown in Fig.12.

In absence of noise and friction, the step response of DP and IE DOF to commands of 10 and 5 degrees are shown in Fig.13. The reference ankle position for DP and IE directions are denoted by r_{DP} and r_{IE}. A pulse shape disturbance of 0.5 Nm was applied to both DOF of the ankle at $t = 2$ *sec* and removed at $t = 3$ *sec*. The corresponding motor torques required to reject the disturbance and follow the step commands are shown in Fig.13b.

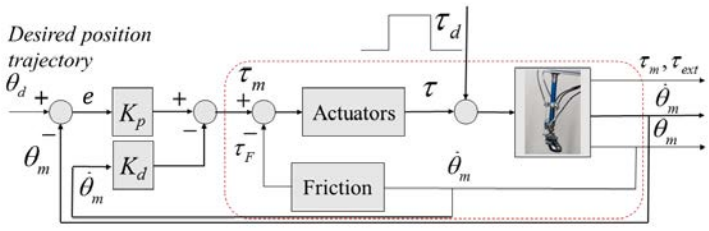

FIGURE 12: Block diagram of the ankle-foot prosthesis model with friction, noise, disturbances and a motor PD controller.

The same simulation was repeated after adding the quantization noise and the Coulomb and viscous friction to the model. Figure 14a shows tracking at the ankle joint with two DOF which have steady state errors.

Figure 14b shows the corresponding torque signals presenting the effects of increased torque due to friction. It also shows the torque ripples due to stiction after t=3 seconds. This effect was investigated by adding and removing stiction from the model. The external disturbance caused more deviation from the reference in IE due to lower stiffness compared to DP axis at the ankle (Fig.14a). The step response simulations are validated experimentally as shown in Fig.15. The experimental results show a good agreement with the simulation predictions. The control signal in Fig.15.b has more noise compared to the simulated response in Fig.14.b. These simulations and experiments were used to guide future designs on the sensor placements needed for

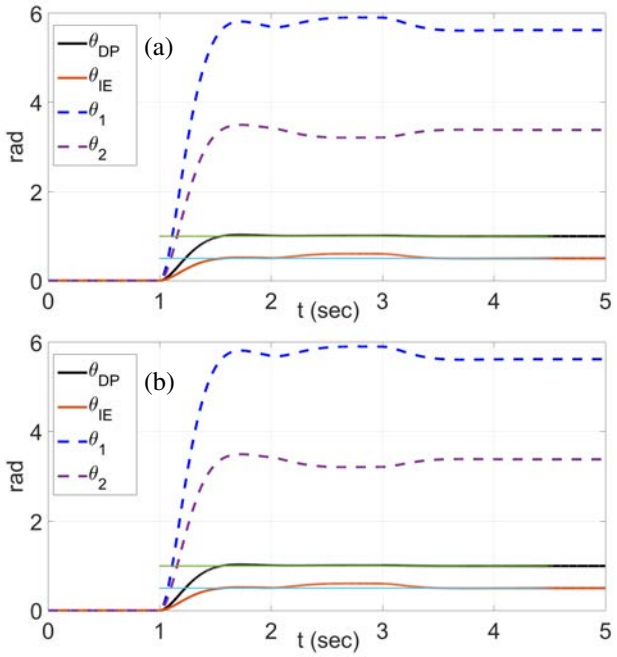

FIGURE 13: Step response of the nominal model without noise and friction but under disturbance. a) Ankle and motor positions and b) the motor torques.

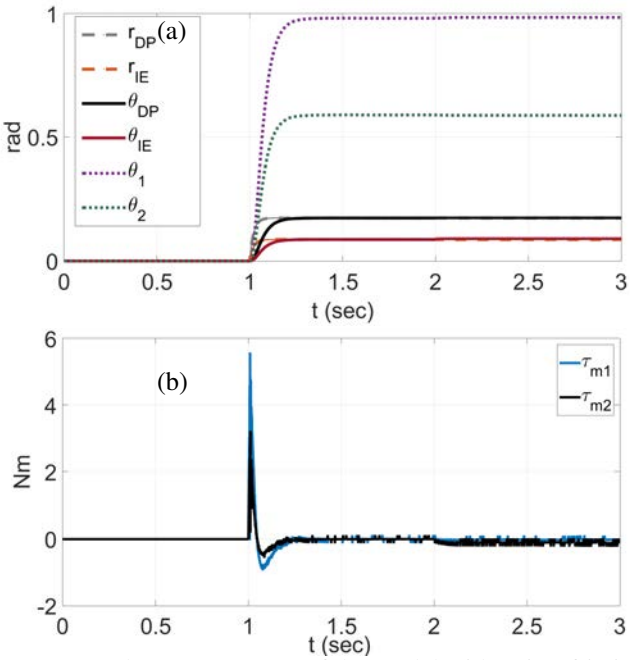

FIGURE 14: The step response of the model with noise, friction, and disturbance. a) Ankle and motor positions and b) the motor torques.

implementation of more advanced controllers that reject external disturbances and compensate for friction loss.

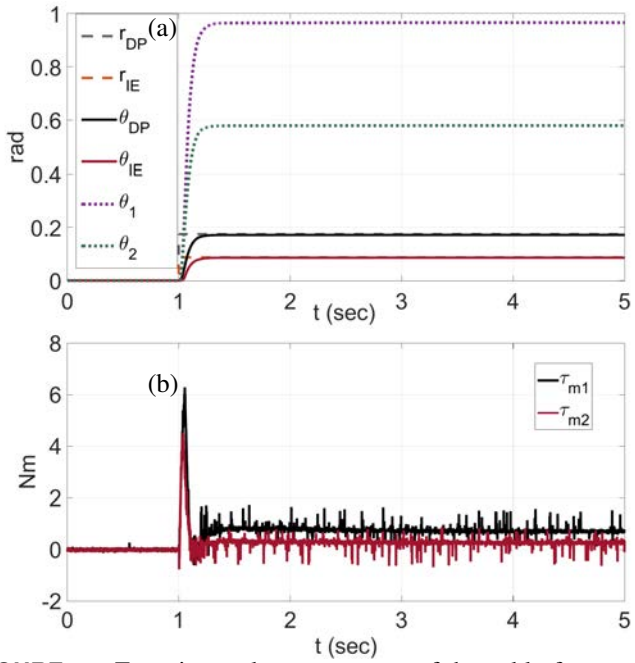

FIGURE 15: Experimental step response of the ankle-foot prosthesis. a) Ankle and motor positions and b) the motor torques.

8 CONCLUSION

In this paper, the authors presented the compliant dynamic model of a recently developed ankle-foot prosthesis. The model parameters were identified using experimental data and the resulting model was validated using additional experiments. Open loop Bode plots were used to study the effect of the pulley radii and cable stiffness on dynamic decoupling of the ankle-foot prosthesis to DP and IE torque commands. Dynamic simulations were used to guide the next design updates on sensor placements to implement advanced impedance control required for the prosthesis.

In future work, the ankle joint can be instrumented with high resolution encoders and force sensors to measure the foot position and force at the foot, providing the means for improved system identification and control.

REFERENCES

[1] Hitt, J., Merlo, J., Johnston, J., Holgate, M., Boehler, A., Hollander, K., and Sugar, T., 2010. "Bionic running for unilateral transtibial military amputees". In 27th Army Science Conference (ASC).

[2] Hitt, J. K., Sugar, T. G., Holgate, M., and Bellman, R., 2010. "An active foot-ankle prosthesis with biomechanical energy regeneration". *Journal of Medical Devices-Transactions of the Asme,* ***4***(1).

[3] College park, 2016. trustep. `http://goo.gl/lGGbDd`.

[4] Össur, 2016. The proprio foot. `http://goo.gl/tfm52l`.

[5] Össur, 2016. The pro-flex foot. http://goo.gl/w7DdPL.

[6] Herr, H. M., and Grabowski, A. M., 2012. "Bionic ankle-foot prosthesis normalizes walking gait for persons with leg amputation". *Proceedings of the Royal Society of London B: Biological Sciences,* ***279***(1728), pp. 457–464.

[7] Hogan, N., 1985. "Impedance control: An approach to manipulation: Part I-theory". *J. Dyn. Sys., Meas., Control,* ***107***(1), pp. 1–7.

[8] Bellman, R. D., Holgate, M. A., and Sugar, T. G., 2008. "Sparky 3: Design of an active robotic ankle prosthesis with two actuated degrees of freedom using regenerative kinetics". In 2nd IEEE RAS & EMBS International Conference on Biomedical Robotics and Biomechatronics (BioRob), pp. 511–516.

[9] Hitt, J. K., Bellman, R., Holgate, M., Sugar, T. G., and Hollander, K. W., 2007. "The sparky (spring ankle with regenerative kinetics) project: Design and analysis of a robotic transtibial prosthesis with regenerative kinetics". In ASME International Design Engineering Technical Conferences and Computers and Information in Engineering Conference, American Society of Mechanical Engineers, pp. 1587–1596.

[10] Ficanha, E. M., Rastgaar, M., Moridian, B., and Mahmoudian, N., 2013. "Ankle angles during step turn and straight walk: Implications for the design of a steerable ankle-foot prosthetic robot". In ASME Dynamic Systems and Control Conference, American Society of Mechanical Engineers, pp. V001T09A001–V001T09A001.

[11] Ficanha, E. M., Rastgaar, M., and Kaufman, K. R., 2015. "Control of a 2-dof powered ankle-foot mechanism". In IEEE International Conference on Robotics and Automation (ICRA), pp. 6439–6444.

[12] Panzenbeck, J. T., and Klute, G. K., 2012. "A powered inverting and everting prosthetic foot for balance assistance in lower limb amputees". *JPO: Journal of Prosthetics and Orthotics,* ***24***(4), pp. 175–180.

[13] Collins, S. H., Kim, M., Chen, T., and Chen, T., 2015. "An ankle-foot prosthesis emulator with control of plantarflexion and inversion-eversion torque". In IEEE International Conference on Robotics and Automation (ICRA), pp. 1210–1216.

[14] Letier, P., Schiele, A., Avraam, M., Horodinca, M., and Preumont, A., 2006. "Bowden cable actuator for torque-feedback in haptic applications". In Proc. Eurohaptics Conf., Paris, July 2006.

[15] Chen, D., Yun, Y., and Deshpande, A. D., 2014. "Experimental characterization of bowden cable friction". In IEEE International Conference on Robotics and Automation (ICRA), pp. 5927–5933.

[16] Spong, M. W., 1987. "Modeling and control of elastic joint robots". *Journal of dynamic systems, measurement, and control,* ***109***(4), pp. 310–318.

[17] Ljung, L., 1987. "System identication: theory for the user". *Englewood Cliffs*.

[18] Armstrong-Hlouvry, B., Dupont, P., and De Wit, C. C., 1994. "A survey of models, analysis tools and compensation methods for the control of machines with friction". *Automatica,* ***30***(7), pp. 1083–1138.

[19] Bram de, J., Maarten, S., and Dragan, K., 2004. *Modeling and Identification for Robot Motion Control*. CRC Press, pp. 268–293.

[20] Dallali, H., 2016. Simulation code for the powered ankle-foot prosthesis. https://github.com/HDallali/HiRo_ankleFootProsthesis.git.